Journal of Alloys and Compounds 513 (2012) 172–179

Contents lists available at SciVerse ScienceDirect

Journal of Alloys and Compounds

journal homepage: www.elsevier.com/locate/jallcom

Glass transition kinetics and radial distribution function to investigate the role of Cr_2O_3 on the structure of Li_2O–Al_2O_3–SiO_2 photonic glass

F.A. Abdel-Wahab [a], Ali Abou Shama [a], Manal Abdel-Baki [b], Fouad El-Diasty [a,*]

[a] Physics Department, Faculty of Science, Ain Shams University, Abbassia, 11566 Cairo, Egypt
[b] Glass Department, National Research Centre, Dokki, 12311 Giza, Egypt

ARTICLE INFO

Article history:
Received 13 September 2011
Accepted 6 October 2011
Available online 17 October 2011

Keywords:
LAS glass
Kinetic parameters
Radial distribution function
Chromium oxide
Band gap

ABSTRACT

Thermal kinetic parameters of Cr_2O_3 doped lithium-aluminum-silicate (LAS) photonic glass are calculated using differential thermal analysis (DTA). The dependence of kinetic parameters together with the glass forming ability of the investigated glass on the Cr_2O_3 doping level showed an anomalous behavior around 0.4 g. Correlation between the obtained thermal properties and the materials electronegativity and band gap is given. An energy band diagram is proposed explaining the density of energy states of Cr^{3+} and its transformation to Cr^{6+}. The non-bridging oxygen bonds generated by Cr_2O_3 produce a deep donor level responsible for the red shift of the absorption edge. The local order structure is studied for the LAS glass network using the radial distribution function of XRD. The atomic pairs of Si–O, Li–O and Si–Si are clearly revealed in both short range (SRO) and medium range (MRO) orders, respectively. The addition of Cr_2O_3 into the glass network has changed appreciably both the atomic pair distances and the coordination numbers in the MRO due to the multivalent nature of Cr ions. The observed decrease in the fourth shell coordination number, N_4, reflects the atomic size decrease in the given glass network which means an increase in glass compactness.

1. Introduction

Lithium aluminum silicate (LAS) glass is known due to their high transparency in the far infrared region and for their relatively moderate density and refractive index. In view of these qualities these glasses are considered as material for optical components such as IR domes, optical filters, modulators, memories, and laser windows. LAS glass ceramic has low thermal expansion coefficient, high heat resistance and excellent mechanical properties [1–3]. The crystallization conditions and proper nucleation agents in the composition of the initial glass are the crucial issues in obtaining high quality and low cost glass ceramic [4–6]. Furthermore, these glasses may be considered as good materials for hosting lasing ions such as chromium/rare-earth ions since these glasses provide a low phonon energy environment to minimize non-radiative losses. In addition, materials which contains mixed valence such as chromium are of recent interest, as cathode materials in rechargeable batteries owing due to their very high energy density and high capacitance [7,8].

Transition metal ions are added to the LAS not only as nucleation or crystallization agents but also to probe the glass structure since their outer *d*-electron orbitals have a broad radial distribution. Ions with $3d^2$ configurations are of interest in solid state laser materials due to their ability to generate laser emission in the near infrared spectral region between 1.2 and 1.7 μm. Owing to "ligand field" theory the energy levels of the 3*d* electrons are split by the electric field of the coordinating ions. Moreover, the *d*-electron orbitals are strongly directional, so the splitting is sensitive to the arrangement of the surrounding ions.

Among various transition metal ions, chromium ion as a paramagnetic ion when dissolved in glass structural matrices in very small amount affects strongly most of its physical properties. This is due to the existence of chromium in two oxidation states, where Cr^{3+} may act as a modifier while Cr^{6+} acts as network former with CrO_4^{2-} structural units [9,10]. Such multiple chromium states that can simultaneously be presented in the glass depend on the modifier–former properties, size of the ions, their field strengths and mobility of the modifier cation.

Recently, we have reported on optical absorption, band gap [11,12], dispersion of nonlinear optical parameters [13] and electrical and dielectric properties [14] of LAS glass system doped with Cr_2O_3. The current investigation studies the dependence of the crystallization kinetics such as crystallization order (n) and activation energy (E_c) together with the glass forming ability on the doping of LAS with Cr_2O_3 in the range of 0.0–0.6 g. The radial distribution function (RDF) of X-ray data is used to investigate the role that Cr^{3+} plays in the LAS structural network changes in both short range order (SRO) and medium range order (MRO), respectively.

* Corresponding author. Fax: +20 2 2682 2189.
E-mail address: fdiasty@yahoo.com (F. El-Diasty).

0925-8388/$ – see front matter © 2011 Elsevier B.V. All rights reserved.
doi:10.1016/j.jallcom.2011.10.014

2. Experimental

Glass system of $13.38Li_2O$–$7.12Al_2O_3$–$79.5SiO_2$ (wt.%) with varying amounts of chromium oxide ranging from 0.0 to 0.6 g are prepared by mixing appropriate weights of raw materials, SiO_2, Li_2CO_3, and Al_2O_3 of purity 5 N, in platinum 2% rhodium crucibles. The amount of the glass batch was 50 g/melt. The mixture is heated in an electric furnace at 1748 K. The duration of melting is 1 h. The synthesis process is continued for a sufficient time to insure complete homogeneity. Then the melt is poured onto a stainless-steel mold and the samples are annealed at temperature (723–773 K). X-ray diffraction confirmed the amorphous nature of the studied glasses [14].

The thermal kinetic parameters or the characteristic glass temperatures such as glass transition (T_g), onset of crystallization (T_0), crystallization maximum (T_p) and melting (T_m) temperatures were determined by differential thermal analysis (DTA). The measurements were performed in an alumina tubular furnace with Cromel–Alumel contact thermocouples using calcinated alumina as the reference material. DTA thermo-grams were recorded in argon atmosphere at heating rate 10 °C/min up to the maximum temperature of 1100 °C using about 0.3 g of the studied glass powders.

The radial distribution data (RDF) of the investigated free and doped LAS glass samples with 0.2, 0.4 and 0.6 g of Cr_2O_3 were collected using Philips (X'pert MPD) diffractometer and the Bragg–Brentano para-focusing technique. Highly monochromatic Cu radiation (wavelength, $\lambda = 1.54051$ Å) was used. The step scan mode was applied in the 2θ-range 4–150°. The step size and the counting time were $\Delta 2\theta = 0.04°$ and 10 s in sequence for each reading. The air scattering was avoided by a suitable applied arrangement of XRD system. The receiving and divergence slits were properly chosen in both small and large 2θ ranges, in order to improve the qualities of data collected.

3. Results and discussion

3.1. Crystallization kinetics

The glass transition is associated with a change from a viscous liquid state to a glassy or structurally arrested state. Therefore T_g is the temperature above which a glassy matrix may attain various structural configurations and below which the matrix is frozen in a thermodynamic quasi stable state [15]. The amount of energy required for movement and rearrangements of atoms around T_g is the activation energy for thermal relaxation. Activation energy of relaxation is basically obtained from the variation of T_g with the heating rate [16]. Accordingly, T_g is related to the cohesive forces (rigidity) within the glassy network those governing the atom movements. Therefore, the glass transition temperature is proportional to material parameters such as the average coordination number, optical band gap, mean bond energy, non-bridging oxygen bonds and average heat of atomization.

The measured thermo-grams of the DTA for un-doped and doped $13.38Li_2O$–$7.12Al_2O_3$–$79.5SiO_2$ glass with 0.2, 0.4 and 0.6 g Cr_2O_3 at a constant heating rate 10 °/min are shown in Fig. 1. This figure shows that each thermo-gram characterizes by a single endothermic peak corresponding to the glass transition temperature, T_g, one exothermic peak denoting crystallization temperature, T_c, and one endothermic peak which reflects value of the melting temperature, T_m. The appearance of single glass transition and single crystallization peaks in the DTA thermo-grams indicates that Cr_2O_3 is homogeneously distributed in the material.

The dependence of the glass transition temperature, T_g, and crystallization peak, T_c, on the Cr_2O_3 doping level for investigated compositions is shown in Fig. 2. A decrease in T_g is seen with the increase in addition of Cr_2O_3. This behavior is a characteristic of the modifying effect of Cr_2O_3 as an ionic oxide on the glass network. It means that the addition of Cr_2O_3 makes glass network more open creating more non-bridging oxygens (NBO). Those NBO are more polarizable than the bridging oxygen bonds which in turn decrease optical band gap of the glass as it will be seen later. On other hand, the crystallization temperature T_c has a non-monotonic trend and shifts towards higher temperatures against the increase in the Cr_2O_3 doping level. In Fig. 2 anomalous point at Cr_2O_3 doping level of 0.4 g for both T_g and T_c is observed.

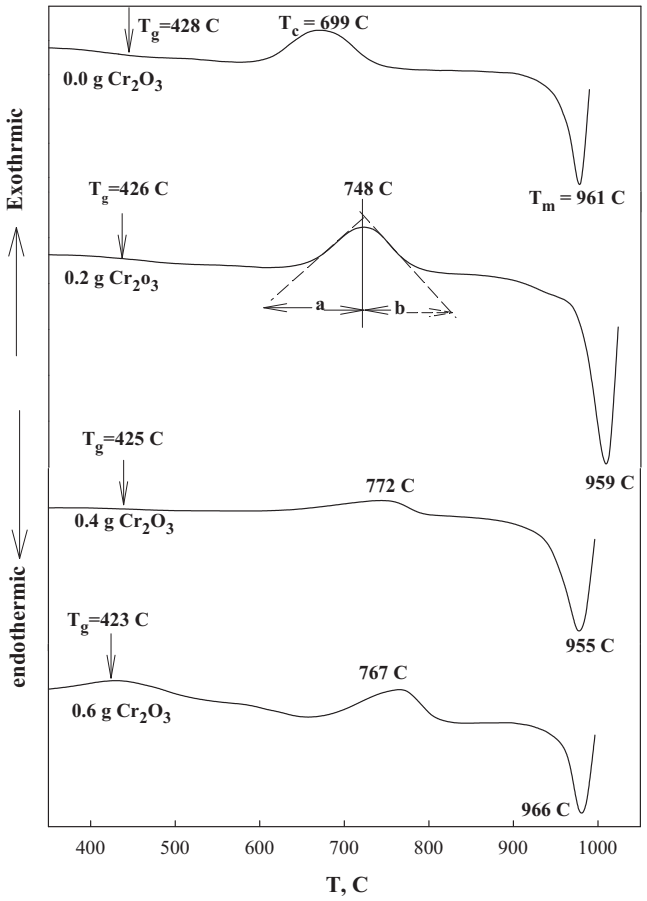

Fig. 1. DTA thermo-grams for the studied free and doped LiO_2–Al_2O_3–SiO_2 with 0.2, 0.4 and 0.6 g of Cr_2O_3 as scanned at constant heating rate 10 °/min.

The fractional volume transformed (i.e., the ratio of the volume of the new phase to the total volume), α, at any temperature T can be determined from the area under the DTA crystallization exothermic curve assuming that α is equal to $A(T)/A(\text{total})$ where $A(T)$ is the partial area up to temperature T and $A(\text{total})$ is the total area under the crystallization curve. The values of $A(T)$ and $A(\text{total})$ are calculated by extracting the experimental data of the crystallization curve and fitting it point by point, for each doping level, to a rational function with fitting parameter $R^2 \approx 0.99$. This fitted function is then

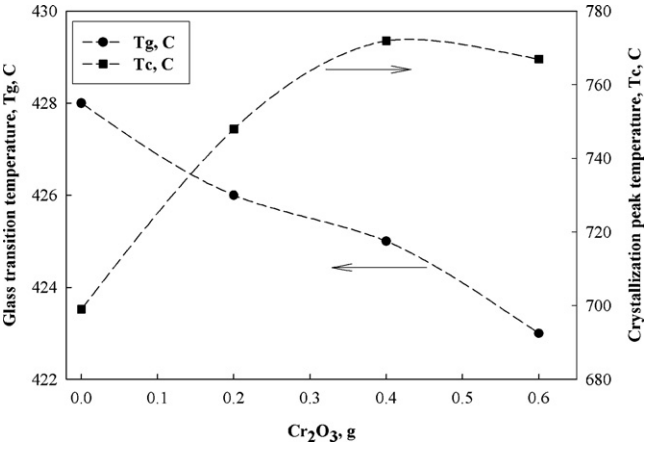

Fig. 2. Dependence of the glass transition, T_g, and crystallization peak, T_c, temperatures on the doping ratio of the present LAS with Cr_2O_3. The dashed lines are only a guide to an eye.

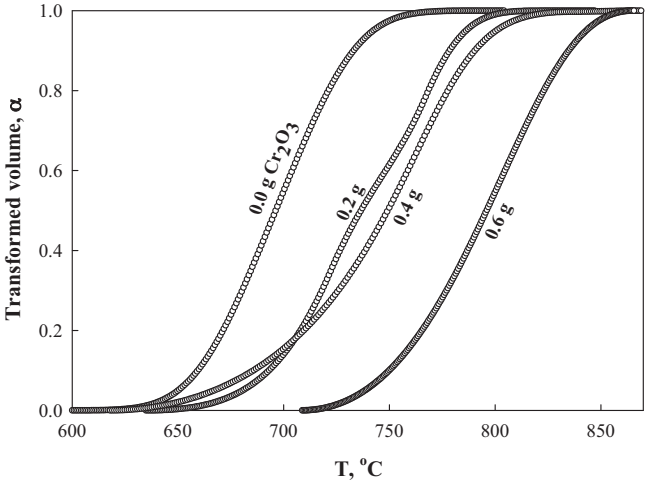

Fig. 3. The transformed fraction, α, for samples under investigation calculated from DTA thermo-grams shown in Fig. 1.

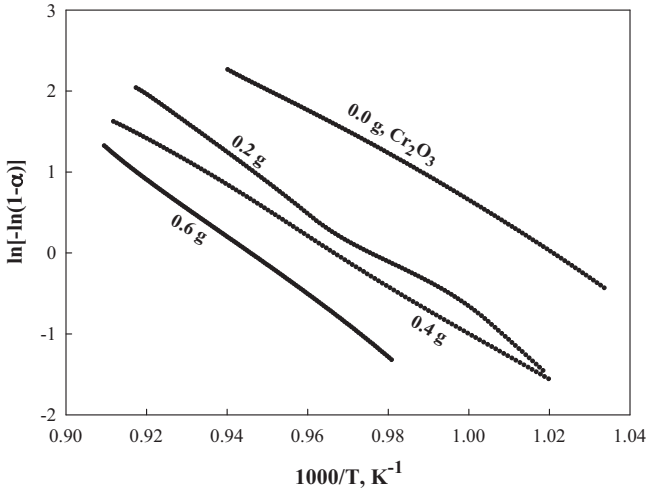

Fig. 4. graphical relation between $\ln[-\ln(1-\alpha)]$ against temperature for present samples.

used to calculate $A(T)$ and $A(\text{total})$ and consequently $\alpha(T)$. Also, this fitted function is solved numerically with the mathematical function representing the base line of the thermo-gram to obtain the initial temperature, T_0 (onset temperature) of the crystallization exothermic peak.

The temperature dependence of the fractional volume transformed, α, at the different doping levels of the studied glass is represented in Fig. 3. Obviously $\alpha = f(T)$ is sigmoid in shape, indicating an autocatalytic reaction as is often observed in various kinds of solid reactions. Also the height of the curve at any temperature is a measure of the temperature difference ΔT between the sample and the reference specimen. This means that the integrated value for the crystallization peak is proportional to the energy required for transition from a less ordered (metastable) to a more ordered (stable) phase.

Activation energy of crystallization is obtained using a method suggested specifically for non-isothermal experiments by Matusita et al. [17]. The volume fraction of crystallites (α) precipitated in a glass heated at constant heating rate (β) is related to the effective activation energy of crystallization (E_c) through the following expression [17],

$$\ln[-(1-\alpha)] = -n\ln\beta - 1.052m\frac{E_c}{RT} \quad (1)$$

where m is an integer which depends on the dimensionality of the crystallization, R is the real gas constant and n being a numerical factor depending also on the nucleation process. In order to investigate dependence of the activation energy of crystallization, E_c, on the doping level of LAS glass with Cr_2O_3 the data are analyzed using Matusita model (Eq. (1)). Fig. 4 illustrates the plot of $\ln[-\ln(1-\alpha)]$ against $1/T$ for different doping levels of Cr_2O_3. The straight lines in this graph are linear fittings according to Eq. (1). From the slope of each straight line, shown in Fig. 4, the mE_c values for undoped and doped LAS glass with Cr_2O_3 are determined.

The reaction order, n, could be obtained, during the amorphous-to-crystalline transformation, using the following Kissinger formula [18]:

$$n = 1.26\left(\frac{a}{b}\right)^{0.5} \quad (2)$$

where (a/b) represents the absolute value of the ratio of the slopes of tangents to the curve at the inflection point of the crystallization peak (see Fig. 1). Applying Eq. (2), the reaction order, n, of the investigated samples could be calculated. Once the value of n is obtained, the effective activation energy E_c can be evaluated at different doping levels. The calculated values of n using Eq. (2) are 1.27, 1.52, 1.74 and 1.69 which corresponds to 0.0, 0.2, 0.4 and 0.6 g, in sequence, of the doping level of LAS glass with Cr_2O_3. Furthermore, calculated values of n show an increase against doping level and reaches its maximum value (=1.74) at 0.4 g of Cr_2O_3 followed by a decrease (=1.69) at 0.6 g. The present values of n illustrates also that doping of LAS with Cr_2O_3 transforms crystallization from one dimension for free LAS ($n = 1.27$) to two dimensions (surface) crystallization for doped LAS with 0.2, 0.4 and 0.6 g.

The calculated values of the activation energy, E_c, as a function of composition for the investigated LAS glass samples are shown in Fig. 5. The general trend of the function is the increase of E_c against the doping concentration and reach its maximum value (=4.69 eV) at 0.4 g Cr_2O_3 followed by a decrease at 0.6 g.

In a given multi-component glass system, there is an obvious correlation between the glass forming ability and composition of that glass. This glass forming ability could be defined as crystallization rate at cooling or at reheating to relaxation process near glass transition [5,19,20], i.e., it depends on the thermal parameters of the studied glass such as transition, onset and crystallization peak

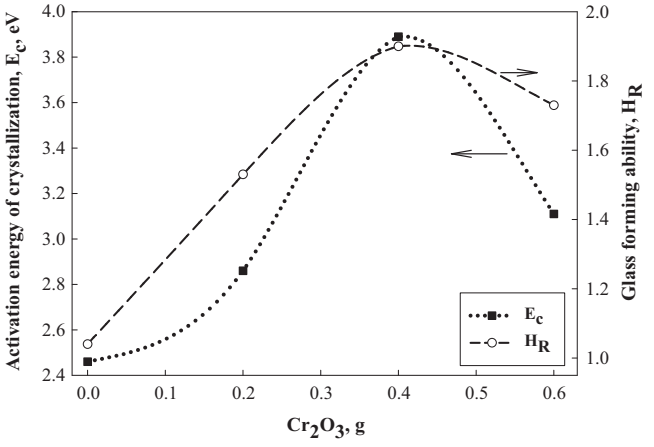

Fig. 5. Activation energy of crystallization, E_c, and glass forming ability, H_R, calculated using Eqs. (1) and (3) in sequence for the investigated samples. The connecting dashed and dotted lines are only a guide to an eye.

temperatures. Hurby [21] suggested a formula for the glass forming ability which is defined as:

$$H_R = \frac{T_c - T_g}{T_m - T_c} \quad (3)$$

Which depends mainly on the difference $(T_c - T_g)$ that could be considered as a thermal nucleation range of the glass. The calculated values of the glass forming ability using Eq. (3) for the investigated doped LAS glasses with Cr_2O_3 are shown in Fig. 5. The glass forming ability, H_R, increases against Cr_2O_3 content and shows an anomalous point at doping level of 0.4 g. Such a behavior is analogous to that reported for different glass systems doped also with different concentrations of Cr_2O_3 such as Li_2–CaF_2–P_2O_5 [22], PbO–Ga_2O_3–P_2O_5 [23] and ZnF_2–ZnO–TeO_2, ZnF_2–CdO–TeO_2, ZnF_2–PbO–TeO_2 [24] and ZnF_2–As_2O_3–TeO_2 [25].

The values of the glass transition, T_g, crystallization peak, T_c, temperatures and glass forming ability H_R are given in Fig. 6 as a function of Cr_2O_3 content for previously published data of different glass systems. The trend shown in Fig. 6(a–c) is the increase (or decrease) against the against Cr_2O_3 content incorporated in the glass network reaching its maximum (or minimum) at a given concentration of Cr ions followed by a reverse in its trend against Cr_2O_3 content. Fig. 6 illustrates also that value of this anomalous point depends on the Cr_2O_3 host glass. For example, the anomalous Cr_2O_3 doping was at 8% for Li_2-CaF_2-P_2O_5 [22], 4% in case of PbO-Ga_2O_3-P_2O_5 [23] and 3% for ZnF_2-PbO-TeO_2 [24] glass systems. Also the same trend is observed with other glasses with different Cr_2O_3 doping percentage for example 1% for ZnF_2-ZnO-TeO_2 [24] and 2% for ZnF_2-CdO-TeO_2 [24].

The anomalous behavior of Cr_2O_3 incorporated with different ratios in different glass systems could be argued to the following: when chromium ion, Cr^{3+}, enters in glass structural matrix in a very small amounts (0.2 g for present work) it acts as a modifier. Thus Cr^{3+} breaks up the local symmetry of the structural network of the glass and introduces coordinated defects known as oxygen dangling bonds or non-bridging oxygen. Increasing the addition of Cr_2O_3 to 0.4 g (present work) increases the concentration of Cr ions where the Cr^{3+} ion losses three electrons to the structural network and transforms to Cr^{6+}. This means that conversion of chromium ions from predominantly Cr^{3+} (d^3) state in octahedral environment to Cr_4^{-2} structural units is occurred. The process of charge transfer between Cr_2O_3 and its host network changes some of the chemical properties such as electronegativity and chemical hardness [26] for the studied LAS glass. The existence of the Cr_4^{-2} structural units causes a decrease in the degree of depolymerization of the glass network. For a chromium addition exceeding 0.4 g, as the case of the present sample 4, a gradual conversion of chromium ions from Cr^{6+} state to Cr^{3+} state exists and the Cr^{3+} ions in such case are acting as modifiers leading to a decrease in the density of non-bridging oxygen bonds (NBO).

Electronegativity, χ, of the constituent oxides alters a lot of physical properties such as optical [12], electrical [11,14] gaps of the studied glasses. The energy gap, E_g, of an oxide can be calculated from the value of its optical electronegativity, $\Delta\chi^*$, using the formula [27–29]:

$$\Delta\chi^* = 0.2688\, E_g \quad (4)$$

where $\Delta\chi^* = \chi_A^* - \chi_C^*$ is the difference between the optical electronegativity of the anion and that of the cation. So the energy gap of the oxide decreases as the optical electronegativity of oxide decreases too. The optical electronegativity of the constituent oxides Li_2O = 1.66 eV, Al_2O_3 = 1.865 eV, SiO_2 = 2.476 eV and Cr_2O_3 = 0.691 eV [30] while their band gap is 6.2 eV, 8.3 eV, 9.1 eV and 3.4 eV [31], respectively. Therefore, since Cr_2O_3 has the lower optical electronegativity (0.691 eV) and the lower band gap (3.4 eV)

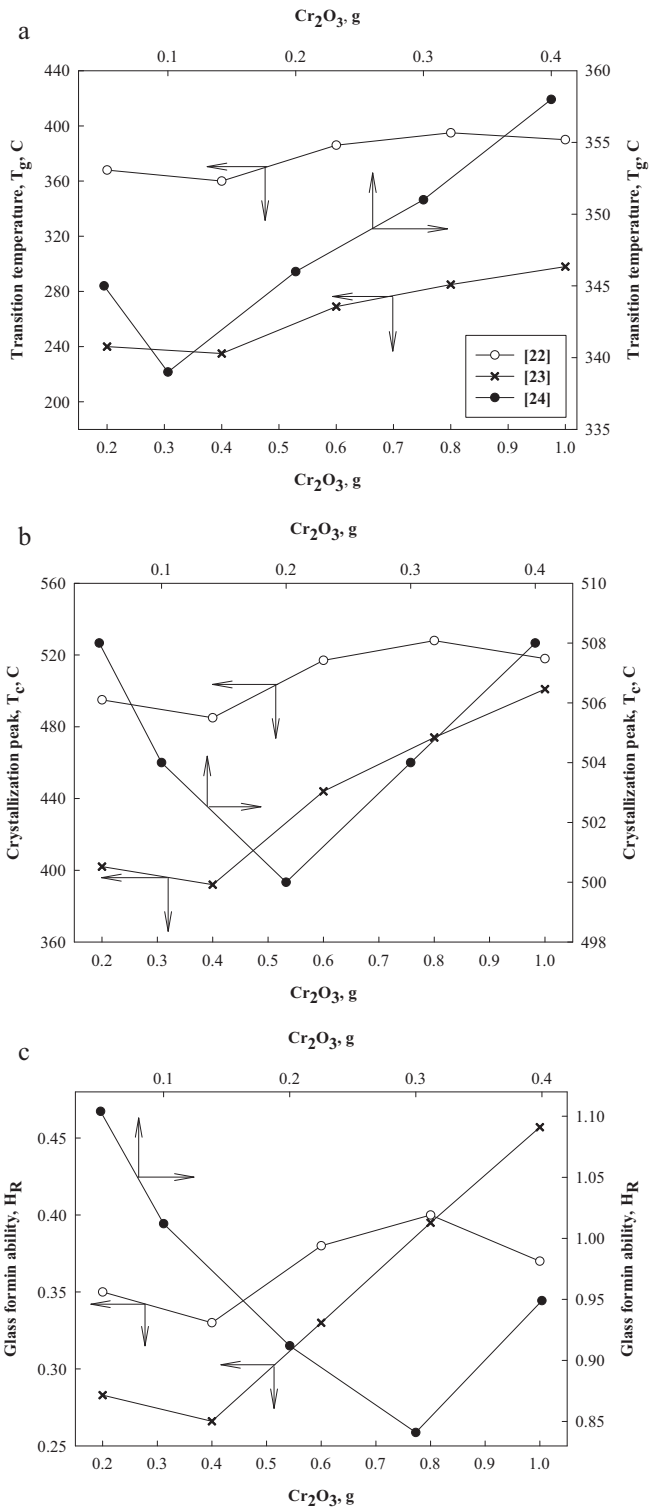

Fig. 6. Dependence of the glass transition, T_g, (a), crystallization peak, T_c, (b) temperatures and glass forming ability, H_R, (c) on the ratio of Cr_2O_3 incorporated in the Li_2O–CaF_2–P_2O_5 [22], PbO–Ga_2O_3–P_2O_5 [23] (lower and left axes) and ZnF_2–ZnO–TeO_2 [24] (upper and right axes). The symbols in figures (b) and (c) has the same meaning as in figure (a). The connecting lines are to show the anomalous points of each composition and also a guide to an eye.

then a reduction in the band gap and glass transition temperature of the studied glass is expected with the addition of Cr_2O_3.

3.2. Molar volume and glass transition temperature

From the microscopic model for glass transition [32], the glass transition temperature for higher coordination number, interplanner spacing and molar volume are related as:

$$kT_g \approx \frac{1}{d^4} \approx \frac{N^{4/3}}{V_m^{4/3}} \quad (5)$$

where kT_g is the thermal energy at glass transition temperature T_g, d is the interplanner spacing, N is the Avogadro number and V_m is the molar volume. Regarding to the molar volume values of our investigated glasses ([12], Table 1 of the present work) and the determined glass transition temperature (Section 3.1) Eq. (5) is fitted will. Such increase in the glass molar volume with the addition of Cr_2O_3 means the formation of non-bridging oxygens leading to excess free volumes and hence decreasing the glass transition temperature as investigated in Section 3.1.

3.3. Glass transition temperature and band gap correlation

The correlation between glass transition temperature, T_g, and band gap energy, E_g, is an essential characteristic relating structure and properties of amorphous materials. The origin of $T_g - E_g$, correlation is based upon the average coordination number, Z (as a chemical bonding aspect) and is given by deNeufville and Rockstad [33] through the relation:

$$T_g = T_g^0 + A[(Z) - 2]E_{04} \quad (6)$$

where A is a linear proportionality constant, $T_g^0 \approx 340 \pm 20^\circ$ and E_{04} is the photon energy at which the optical absorption coefficient has the value of $10^4\,cm^{-1}$. The equation indicates that there is a direct proportion between glass transition and the band gap energy. According to the previously published data on the indirect band gap energy values for undoped and Cr_2O_3-doped LAS glasses which is extracted from Ref. [12] and inserted in Table 1, a decrease in the band gap is occurred with the increase in the addition of Cr_2O_3. Such result confirms and explains in the same time the obtained decrease in the glass transition temperature with band gap energy and the role of Cr_2O_3 addition on LAS glass transition kinetics.

3.4. XRD radial distribution function

The structure of multicomponent oxide glasses is poorly understood where the lack of periodicity means that it would be necessary to specify the coordinates of every atom present, which is impossible for a real glass. Traditionally, there have been two approaches to the formation of glasses: the conventional formalism, as specified by diffraction studies, and the chemical description, as employed by Shultz et al. [34].

The conventional formalism is represented by the crystallite and random network theories, which extend the ideas of crystallography to the vitreous state and discuss the structure in terms of atomic coordinates, bond lengths, and angles. The chemical description, on the other hand, considers a glass to be the result of chemical reactions and, hence, its structure to be composed of chemical groupings. In the present study, RDF technique is used to investigate the glass structure because oxide glasses are mainly isotropic on a macroscopic scale and the maximum that can be extracted from a diffraction experiment is a one-dimensional correlation function.

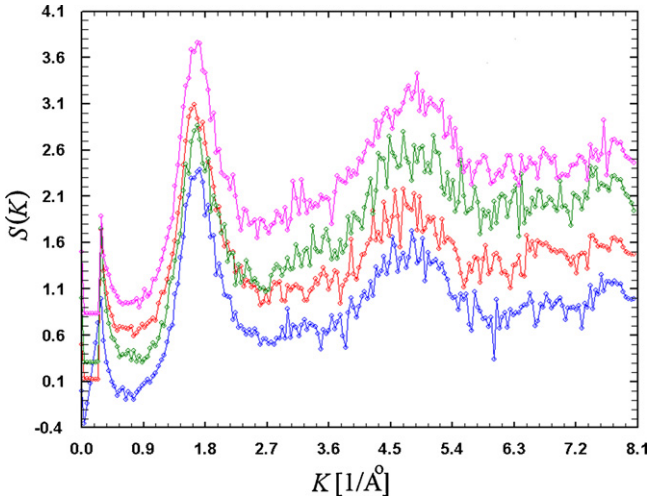

Fig. 7. Structure factor, $S(K)$, as function of K for the present LAS compositions. The doping level increase from bottom to top.

The total structure factor of a glass is given as

$$S(K) = \frac{\{I(K) - [\langle f^2\rangle - \langle f\rangle^2]\}}{\langle f\rangle^2} \quad (7)$$

where $I(K)$ is being the scattered corrected X-ray intensity of the atomic species constituting the given specimen, f is the atomic scattering factor. $K = 4\pi\sin\theta/\lambda$ is the magnitude of the scattering vector. The term $[\langle f\rangle^2 - \langle f\rangle^2]$ is known as the Laue diffraction. This Laue term is of more significance at small angle (2θ) of scattering. The observed $S(K)$ is related to the deviation from the average number density ρ_0 by a sine transform as

$$S(K) = \frac{4\pi}{K\int_0^\infty r[\rho(r) - \rho_0]\sin(Kr)dr} \quad (8)$$

where $\rho(r)$ is the atomic density as a function of the radial distance r. Here

$$\rho_0 = \frac{\rho N}{A \times 10^{24}} \quad (9)$$

where ρ is the sample density in gm/cm^3, N is the Avogadro's number, A is being the sample atomic weight. RDF is given as

$$4\pi r^2\rho(r) = rG(r) + 4\pi r^2\rho_0 \quad (10)$$

where $G(r)$ is the reduced RDF, so

$$G(r) = 4\pi r[\rho(r) - \rho_0] = \frac{2}{\pi}\int_0^\infty K[S(K) - 1]e^{-\alpha^2K^2}\sin(Kr)dK \quad (11)$$

$4\pi r^2\rho_0$ is of asymptotic form and α^2 is the disordering parameter of value $\approx 0.01\,Å^2$ mainly used to reduce the effect of spurious details in the high K-range in the measured data.

During the X-ray run of all the investigated samples, the collected intensity is corrected for the polarization, absorption and background [35,36]. To focus our study on local order structure of the studied glasses, the corrected intensity was normalized in order to convert it into electron units (e.u.) resulting finally on the structure factor $S(K)$ with a corresponding accessible maximum scattering vector magnitude, K, $8.0\,Å^{-1}$.

Fig. 7 shows $S(K)$ versus K for the investigated LAS glass with the addition of 0.0, 0.2, 0.4 and 0.6 g of Cr_2O_3 respectively. The two main prominent peaks of $S(K)$, appeared for all samples, in the reciprocal space are centered at 1.68 and $4.85\,Å^{-1}$ with a broadening in the second peak which may have a more than one resolved peak. A

Table 1
Hydrostatic density, D, molar volume, V_m, glass transition, T_g, and crystallization, T_c, temperatures, indirect optical gap, E^g_{ind}, Si–O–Si bond angle, Φ and tail states as function composition of the studied glass.

S	Glass composition (wt.%)	D (g/cm^3) [12]	V_m (cm^3 mol^{-1}) [12]	T_g (°C) (PW)	T_c (°C) (PW)	E^g_{ind} (eV) [12]	Φ (Si–O–Si) (PW)	E_u (eV) [12]
1	13.38Li_2O–7.12Al_2O_3–79.5SiO_2	2.33	25.3	428	699	3.46	128.99	0.804
2	13.38Li_2O–7.12Al_2O_3–79.5SiO_2 + 0.2 g Cr_2O_3	2.37	25.0	426	748	2.66	135.48	0.197
3	13.38Li_2O–7.12Al_2O_3–79.5SiO_2 + 0.4 g Cr_2O_3	2.38	25.03	425	772	2.62	121.78	0.195
4	13.38Li_2O–7.12Al_2O_3–79.5SiO_2 + 0.6 g Cr_2O_3	2.39	25.05	423	767	2.48	131.53	0.197

PW, present work.

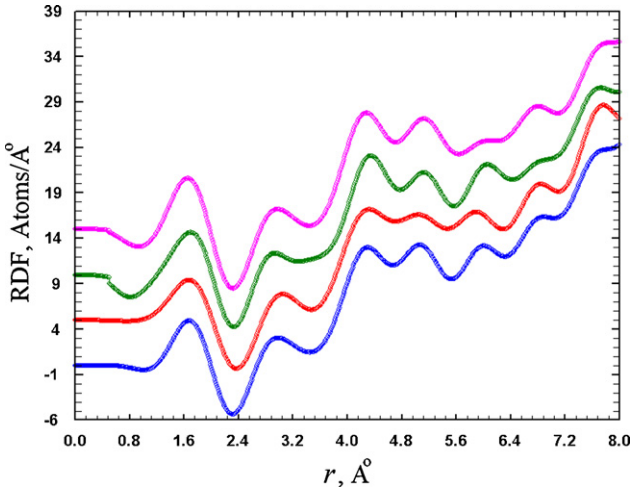

Fig. 8. Radial distribution function, RDF, as a function of r for the LAS compositions. The doping level increase from bottom to top.

third small intense resolved peak is observed also for all the studied samples at about 7.7 Å^{-1}. As one can view the signal to noise ratio is good and the first peak (at 1.68 Å^{-1}) is of small broadening compared to the other peaks indicating the good ordered peaks of Si–O correlations. Another small peak is observed at 6.7 Å^{-1} for samples one, two and four (having 0.0, 0.2, and 0.6 g Cr_2O_3 in sequence). Other two peaks centered at 3.25 Å^{-1} and 3.48 Å^{-1} (as a shoulder) are detected for samples 3 and 4.

Fig. 8 illustrates the dependence of the radial distribution function (RDF) on the radial distance r for the different glass compositions. The actual introduced weights of the main components are: 24.3 Li_2O–3.8 Al_2O_3–71.9 SiO_2, accordingly the correlated pairs will be due to Si–O, Si–Si, Li–O and/or Li–Li pairs. The first peak in RDF spectrum which belongs to Si–O atomic pairs in the considered samples, more or less, is located at the same position ~1.65 Å, except the third sample having an elongated correlation distance at 1.69 Å. This peak refers to another atomic pairs of Li–O at a distance of about 2.18 Å. The coordination number of this first peak (~1.65 Å) is on average 7.39 which means that both of Si–O and Li–O are of tetrahedral nature in form of SiO_4 and LiO_4 respectively. These atomic pairs of Si–O and Li–O are previously detected in the infrared absorption spectrum of LAS glass [12]. The Si–O and Li–O pairs which represent the source of non-bridging oxygen give shallow defect states near the top of the valence band edge of the studied glass. These defect states act as hole traps [37]. As stated above, increasing the value of the incorporated Cr_2O_3 up to 0.4 g increases non-bridging oxygen which in turn increases the concentration of the atomic pairs Si–O and Li–O and consequently increasing the density of these hole trap states [38].

The second coordination shell for the first (un-doped) and the fourth (0.6 g Cr_2O_3) glass samples is detected at the same distance, 2.974 Å, while for the second sample, this peak was shifted to 3.05 Å and in the third one it is shifted to 2.93 Å. This second RDF peak belongs to the distorted Si–Si correlations arranged in form of distorted tetrahedral units of an average coordination number 4.0. This second peak is also of composite structure having a small contribution of Li–Li pairs. The high stretching of the second peak, for the second sample, is due to the introduction of Cr_2O_3 which could be considered as an indication to the increased order in the medium range structure in the glass network of the LAS system. Also, the observed shortening of the same peak in the third sample (0.4 g Cr_2O_3) is an indicative way to the high ordering of the atomic pairs observed in the short range order (SRO), resulting in their good stability [11,12].

The third observed peak for the investigated LAS glass system is detected at 4.22 Å for the un-doped sample which belongs to Si–O second order shell correlations having a building unit as SiO_4 and Li–O pairs having the form of LiO_6 octahedral form. As it can be seen, with the addition of Cr_2O_3 to the glass network, the third peak is shifted to a longer radial distance r which reveals the increase of order in the medium range structure of these samples. This structural modification inside medium range order (MRO) of the LAS glass system is mainly due to the presence of Cr^{3+} ions (as a modifier) and the evolution of non-bridging oxygen connected with both Si and Li atoms as reported by El-Diasty et al. [11,12]. The same third peak is again shifted to ~4.28 Å in sample 4 which is shorter by about 0.06 Å compared to the previous two doped samples (having r_3 at 4.33 Å). This shifting in r_3 towards smaller values is an indication to the LAS glass stability in the SRO network units. The absence of other pairs such as Al–O and Cr–O may be due to their small introduced percents inside the LAS glass network. Table 2 shows the first RDF peak positions and coordination numbers with the concentrations for Cr, Li, Al, Si and O, respectively.

Concerning the bond angle distributions of Si–O–Si, one can observe that, with the introduction of Cr_2O_3 in the LAS network this angle is enhanced from 140.58° (un-doped sample) to ~148° in sample 2 and 4. These Si–O–Si connected pairs are good relaxed in the third sample (containing 0.4 g Cr_2O_3) compared to other samples to be 132.41°. More or less, the change of Si–O–Si and Li–O–Li bond angles as a function of Cr content having the same trend for the investigated LAS glass and the more relaxed angle for both is 119.12° and 121.776°, respectively, in the MRO which is accompanied by a contracted bond length of 2.921 Å due to Si–Si correlations. In contradiction, the more distorted angle for Si–O–Si and Li–O–Li angles is observed having 132.572° and 135.482° respectively for the second sample. It is known that the bond angle fluctuation is a common disordered phenomena in glass network and also could be considered as a major reason for presence of the band gap tail states and the variation of the glass transition temperature, T_g, in the investigated LAS glass system (see Table 1) [12].

An extraneous change in the RDF parameters is noted in Table 2 for sample 3. This change may be dominantly occurred due to the introduction of Cr-ions as a modifier in the network besides the presence of Li-ions as another source of parent modifier, but with less effect as compared with the Cr ions. The maximum change of the structure of the SRO and MRO of the network obtained when

Table 2
First RDF peak positions and their coordination numbers with the applied elemental atomic concentrations.

Sample no.	R_1 (Å)	N_1	R_2 (Å)	N_2	R_3 (Å)	N_3	R_4 (Å)	N_4	Cr%	Li%	Al%	Si%	O%	ρ°At/Å^3
1	1.662	7.22	2.974	5.50	4.222	10.21	5.056	10.15	0.00	0.063	0.038	0.371	0.529	0.0270
2	1.664	8.17	3.047	5.39	4.323	9.85	5.051	8.41	0.036	0.059	0.036	0.351	0.518	0.0249
3	1.694	6.78	2.921	4.20	4.340	10.57	5.118	7.77	0.066	0.056	0.032	0.318	0.548	0.0226
4	1.645	7.40	2.974	5.18	4.279	9.86	5.118	9.62	0.102	0.054	0.032	0.316	0.496	0.0226
Pair type	Si–O and Li–O		Si–Si and Li–Li		Si–O and Li–O of order 2				Cr content increases and almost all other elements decreases					

$R = \pm 0.03$ Å, $N = N \pm 0.25$.

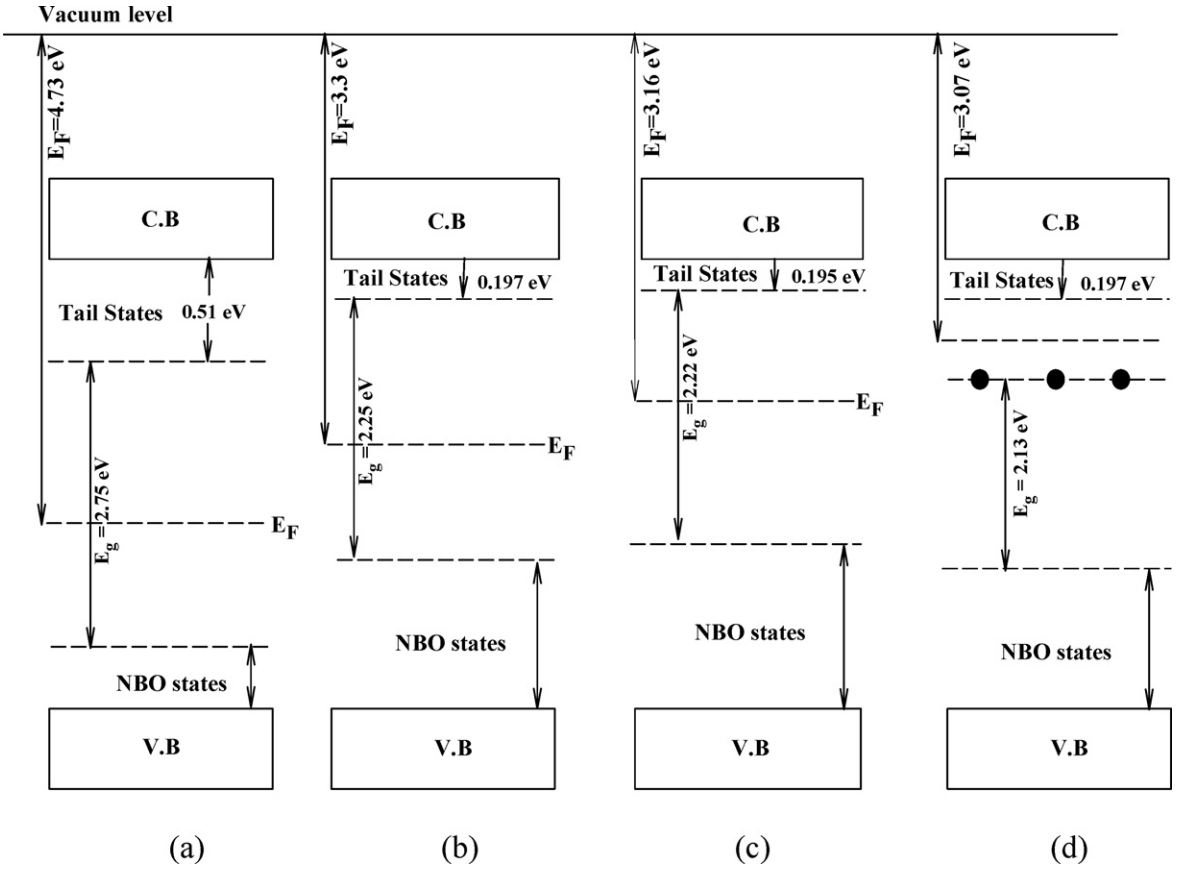

Fig. 9. Proposed energy band diagram of investigated undoped (a), doped with 0 2 g (b), 0.4 g (c) and 0.6 g (d) LAS glass with Cr_2O_3.

Cr_2O_3 is 0.4 g and before this percent and after it the role of Cr ions is of minor effect as a modifier.

The reduction occurred in the coordination number of the fourth peak especially in sample 2 and 3 (column of N_4 in Table 1) is mainly due to the introduction of Cr_2O_3 and the chromium valence change of Cr^{6+} to Cr^{3+} having a modifying network nature [11,12]. As can be observed also in Table 2, N_3 suffers a small decrease in both sample 2 and 4 compared to sample 1 and 3. This decrease in both N_4 and N_3 in the MRO will give an indication to the decrease in the size of the corresponding coordination shells which in turn results in the overall decrease of the glass molar volume as reported in Refs. [9,10]. Another important observation is the modifying effect of Li_2O component which is presented with an appreciable percent of 24.3%.

In view of the above discussion, Fig. 9 illustrates the proposed electronic band gap diagram for the studied Cr_2O_3 contained LAS glass. In case of un-doped composition (Fig. 9a) the states above the top of the valence band (VB) which is argued to un-satisfied Si–O and Li–O bonds, as structural defect, and the role that they plays as a modifier in the structural network of LAS glass. Adding of Cr_2O_3 with 0.2 and 0.4 g (Fig. 9(b) and (c)) creates Cr^{3+} ions which acts as modifier and breaks the symmetry of the glass network and increases the concentration of the NBOs and also its density of states. The negative charges on the NBOs have larger magnitude than that on the bridging oxygens. This conversion from bridging to non-bridging oxygen increases the ionicity of oxygen ions, increasing the density of states above the valence band, and reduces band gap energy [39]. The increase of density of states (DOS) above the valence band (V.B) causes a moving of the Fermi level up word towards the conduction band (C.B) bottom. More addition of Cr_2O_3 above 0.4 g causes Cr^{3+} ions to oxidize by losing three electrons and transforms to Cr^{6+} which acts as network former and decreases the concentration of NBO and its DOS above the top of the VB. The energy level of the three electrons, due to oxidation of Cr^{3+} to Cr^{6+}, takes place at a state below the bottom of the CB as in Fig. 9(d). Both the states above the valence band, due to unsatisfied Si–O and Li–O, and that of the three electrons, due to oxidation of Cr^{3+} to Cr^{6+}, which lie just below the conduction band decreases the activation energy of conduction, ΔE, and consequently increase the dc conductivity against the increase of Cr_2O_3 [14]. The Fermi level, energy gap and tail states values for the considered LAS glass are taken from Ref. [12].

4. Conclusion

Adding of Cr_2O_3 as a transition metal to the Li_2O–Al_2O_3–SiO_2 photonic (LAS) glass in the range of 0.0–0.6 g causes a decrease of the glass transition temperature, T_g, increase of both crystallization peak temperature, T_c, and glass forming ability. Furthermore, the dependence of T_g, T_c and glass forming ability on the concentration of Cr_2O_3 showed an anomalous point at doping level of 0.4 g. This is argued to presence of Cr ions as Cr^{3+} and Cr^{6+} before and after the anomalous concentration. The Cr^{3+} ions in such case are acting as modifiers increasing the concentration of non-bridging oxygen (NBO). The state density of NBO lies above the valence band edge. Increasing Cr_2O_3 to 0.6 g makes Cr^{3+} to loss three electrons and oxidize to Cr^{6+}. The energy states of these three electrons lies just below bottom of the conduction band. These states above and below valence and conduction bands in sequence increase the dc conductivity against Cr_2O_3 [14]. The existence of Al ions may connect the Si–O and Li–O pairs inside the glass network. The shortening of both r_2 (sample 3; 2.921 Å) and r_3 (sample 4; 4.279 Å) is mainly due to the introduction of Cr_2O_3 forming non-bridging oxygen bonds in the glass network. The MRO structure is going towards more order with the increase of Cr_2O_3 content as observed in r_4 for samples 3 and 4. Another important observation in r_4 is the decrease in its coordination number which may be due to the evolution of NBO. The shortening of r_2 (Si–Si pairs) compared to its theoretical value is due to role of Cr_2O_3 and is also due the increase in the compactness of glass network. The obtained results are important for glass laser industry.

References

[1] X.Z. Guo, H. Yang, M. Cao, J. Non-Cryst. Solids 351 (2005) 2133.
[2] X.Z. Guo, H. Yang, C. Han, F.F. Song, Thermochim. Acta 444 (2006) 201.
[3] X.Z. Guo, H. Yang, C. Han, F.F. Song, Ceram. Int. 33 (2007) 1375.
[4] J.H. Perepezko, Prog. Mater. Sci. 49 (2004) 263.
[5] P.W. Mcmilan, Glass–Ceramics, Academic Press, 1979.
[6] A.M. Hu, K.M. Liang, F. Zhou, G.L. Wang, Ceram. Int. 31 (2005) 11.
[7] B.M. Casari, E. Wingstrand, V. Langer, J. Solid State Chem. 179 (2006) 296.
[8] R.P. Ramasamy, P. Ramadass, B.S. Haran, B.N. Popov, J. Power Sources 124 (2003) 155.
[9] O. Guldal, C. Apak, J. Non-Cryst. Solids 38 and 39 (1980) 251.
[10] G. Fuxi, D. He, L. Huiming, J. Non-Cryst. Solids 52 (1982) 135.
[11] F. El-Diasty, M. Abdel-Baki, F.A. Abdel Wahab, H. Darwish, Appl. Opt. 45 (2006) 7818.
[12] F. El-Diasty, F.A. Abdel Wahab, M. Abdel-Baki, J. Appl. Phys. 100 (2006) 093511.
[13] F.A. Abdel Wahab, F. El-Diasty, M. Abdel-Baki, Phys. Lett. A 373 (2009) 3855.
[14] F.A. Abdel Wahab, M. Abdel-Baki, J. Non-Cryst. Solids 355 (2009) 2239.
[15] M.H.R. Lankhorst, J. Non-Cryst. Solids 297 (2002) 210.
[16] N. Mehta, A. Kumer, J. Optoelectron. Adv. Mater. 7 (2005) 1473.
[17] K. Matusita, T. Konatsu, R. Yokota, J. Mater. Sci. 19 (1984) 291.
[18] H.E. Kissinger, Anal. Chem. 29 (1957) 1702.
[19] L.A.P. Maqueda, J.M. Criado, J. Malek, J. Non-Cryst. Solids 320 (2003) 84.
[20] M. Saad, M. Poulain, Mater. Sci. Forum 19–20 (1987) 11.
[21] A. Hurby, Czech. J. Phys. 22 (1972) 1187.
[22] G. Murali Krishna, Y. Gandhi, N. Venkatramaiah, R. Venkatesan, N. Veeraiah, Physica B 403 (2008) 702.
[23] G. Little Flower, M. Srinivasa Reddy, G. Sahaya Baskaran, N. Veeraiah, Opt. Mater. 30 (2007) 357.
[24] C. Laxmi Kanth, B.V. Raghavaiah, B. Appa Rao, N. Veeraiah, J. Quant. Spectrosc. Radiat. Trans. 90 (2005) 97.
[25] D.K. Durga, N. Veeraiah, Physica B 324 (2002) 127.
[26] S.F. Matar, G. Campet, M.A. Subramanian, Prog. Solid State Chem. 39 (2011) 70.
[27] J.A. Duffy, J. Phys. C 13 (1980) 2979.
[28] R.R. Reddy, Y.N. Ahmmed, Cryst. Res. Technol. 30 (1995) 263.
[29] R.R. Reddy, Y.N. Ahmmed, K.R. Gopal, D.V. Raghuram, Opt. Mater. 10 (1998) 95.
[30] R.R. Reddy, K.R. Gopal, K. Narasimhulu, L.S. Sanakara Reddy, K.R. Kumar, C.V. Krishna Reddy, S.N. Ahmed, Opt. Mater. 31 (2008) 209.
[31] J. Portier, H.S. Hilal, I. Saadeddin, S.J. Hwang, M.A. Subramanian, G. Campet, Prog. Solid State Chem. 32 (2004) 207.
[32] P.K. Thiruvikraman, Bull. Mater. Sci. 29 (2006) 371.
[33] J.P. deNeufville, H.K. Rockstad, in: J. Stuke, W. Brening (Eds.), Amorphous and Liquid Semiconductors, Taylor and Francis, London, 1974, p. 419.
[34] B.A. Shakhmatkin, N.M. Vedishcheva, M.M. Shultz, A.S. Wright, J. Non-Cryst. Solids 177 (1994) 249.
[35] J. Krogh-Moe, J. Non-Cryst. Solids 1 (1969) 269.
[36] R.L. Mozzi, B.E. Warren, J. Appl. Crystallogr. 3 (1970) 251.
[37] M. Stapelbroek, D.L. Griscom, E.J. Friebele, G.H. Sigel Jr., J. Non-Cryst. Solids 32 (1979) 313.
[38] S. Lin, Comput. Mater. Sci. 23 (2002) 80.
[39] J.A. Duffy, Phys. Chem. Glasses 42 (2001) 151.